AIP | Journal of Applied Physics

Towards quantitative off-axis electron holographic mapping of the electric field around the tip of a sharp biased metallic needle

M. Beleggia, T. Kasama, D. J. Larson, T. F. Kelly, R. E. Dunin-Borkowski, and G. Pozzi

Citation: Journal of Applied Physics **116**, 024305 (2014); doi: 10.1063/1.4887448
View online: http://dx.doi.org/10.1063/1.4887448
View Table of Contents: http://scitation.aip.org/content/aip/journal/jap/116/2?ver=pdfcov
Published by the AIP Publishing

Towards quantitative off-axis electron holographic mapping of the electric field around the tip of a sharp biased metallic needle

M. Beleggia,[1,2] T. Kasama,[1] D. J. Larson,[3] T. F. Kelly,[3] R. E. Dunin-Borkowski,[4] and G. Pozzi[5]
[1]*Center for Electron Nanoscopy, Technical University of Denmark, Kongens Lyngby, Denmark*
[2]*Helmholtz-Zentrum Berlin für Materialien und Energie, Berlin, Germany*
[3]*CAMECA Instruments, Inc., Madison, Wisconsin 53711, USA*
[4]*Ernst Ruska-Centre for Microscopy and Spectroscopy with Electrons and Peter Grünberg Institute, Forschungzentrum Jülich, Jülich, Germany*
[5]*Department of Physics and Astronomy, University of Bologna, Bologna, Italy*

(Received 27 March 2014; accepted 25 June 2014; published online 10 July 2014)

We apply off-axis electron holography and Lorentz microscopy in the transmission electron microscope to map the electric field generated by a sharp biased metallic tip. A combination of experimental data and modelling provides quantitative information about the potential and the field around the tip. Close to the tip apex, we measure a maximum field intensity of 82 MV/m, corresponding to a field k factor of 2.5, in excellent agreement with theory. In order to verify the validity of the measurements, we use the inferred charge density distribution in the tip region to generate simulated phase maps and Fresnel (out-of-focus) images for comparison with experimental measurements. While the overall agreement is excellent, the simulations also highlight the presence of an unexpected astigmatic contribution to the intensity in a highly defocused Fresnel image, which is thought to result from the geometry of the applied field. © *2014 AIP Publishing LLC*.
[http://dx.doi.org/10.1063/1.4887448]

I. INTRODUCTION

The concept of a laboratory in a transmission electron microscope (TEM) describes a combination of high-resolution analytical techniques with experiments that are traditionally carried out *ex situ*.[1] Here, we focus on the investigation of a sharp metallic tip, such as that used in field-electron emission and field evaporation, using *in situ* electrical biasing, off-axis electron holography, and Fresnel (out-of-focus) imaging in the TEM, in combination with theoretical modeling. The quantitative measurement of the electrostatic field topography around a biased tip is of great importance to the field-emission and atom probe communities, as the fundamental question of how the electrostatic field interacts with a metallic needle has not yet been addressed adequately.[2] Furthermore, a knowledge of the electrostatic field topography around the tip apex may form the basis of an aberration correction scheme for atom probe tomography (APT),[3,4] which could lead to the realization of atomic-scale tomographic measurements.[5]

APT achieves high spatial resolution, on the order of 150 pm,[6] in those parts of images where trajectory aberrations are not large,[7] e.g., in single phase materials close to, but not at, low index poles. However, when aberrations degrade the recorded image, the local spatial resolution can be reduced to a few nanometers due to reconstruction errors associated with a lack of knowledge of the true ion trajectories. Imaging in APT is based on a projection, such that the faithful reconstruction of atom positions depends on the accuracy of the projection used and is most successful when the specimen apex varies smoothly and follows a known shape. However, when the apex has topological features that are not known, simple projection laws will be incorrect and the resulting "aberrations" will limit the spatial resolution of the technique. In this way, the specimen shape (and its dielectric properties) determine the electrostatic field topography around the specimen apex, which, in turn, determines the ion trajectories towards the imaging detector.[8]

The electrostatic field topography around a sharp tip has been modeled analytically.[9] However, this type of model is known to be a simple approximation. Although more accurate models can be computed using boundary element methods, it is challenging to accommodate the several orders of magnitude in length scale that span the nanometer-dimensions of the specimen apex and the millimeter-scale of the detector. Despite these difficulties, commercial boundary element method programs can be used successfully for this purpose, so long as the specimen shape is available as input.[10]

Measurement of the specimen apex shape has been identified as the basis for correcting image aberrations in atom probe tomography.[5] Alternatively and equivalently, a knowledge of the electrostatic field topography about the specimen apex can form the basis of reconstructing raw hit data into aberration-corrected images. The spatial resolution of the measured electrostatic field topography about the apex would need to be on the order of 1 nm if there is to be value in determining it for correcting aberrations. In this paper, we demonstrate an approach that can be used to perform such a measurement.

We first present results obtained using off-axis electron holography and Fresnel (out-of-focus) imaging in the TEM. The experiments involve electrically biasing a metallic tungsten (W) tip *in situ* in the TEM. We then introduce a model for the electrostatic field around the biased tip, which we develop using basic electrostatics. Image simulations based

on this model are compared to the experimental measurements, allowing the charge density distribution in the tip region to be determined. The soundness of the procedure and the accuracy of the measured charge density distribution are assessed by inserting the measured values as input into simulations of out-of-focus images. Satisfying agreement with experimental out-of-focus images is obtained if an unexpected astigmatic contribution to the phase shift, which is thought to result from the geometry of the applied field, is taken into account.

II. EXPERIMENTAL DETAILS AND RESULTS

A metallic tip was prepared by thinning a W wire using standard electrochemical methods. The terminal part of the wire, about 1.5 mm long, was cut and crimped into an Omniprobe Cu TEM half-grid. This specimen was inserted into an ultra-high-tilt three-contact cartridge-based specimen holder designed by E.A. Fischione Instruments, Inc.,[1,11] in which a counter-tip could be moved to a desired position using a piezo-controlled stage and biased using an external voltage source, as shown in Fig. 1(a).

Off-axis electron holography is used to characterize magnetic and electrostatic fields arising from structures of interest in the TEM at a spatial resolution that can approach or exceed 1 nm. The technique[12–14] involves applying a positive voltage to an electron biprism,[15] in order to overlap a coherent electron wave that has passed through a sample with a part of the same electron wave that has passed only through vacuum, as shown in Fig. 1(b).

In principle, analysis of the resulting interference pattern allows the phase shift of the object wave

$$\varphi(x,y) = C_E \int_{-\infty}^{\infty} V(x,y,z)\mathrm{d}z \qquad (1)$$

to be recovered quantitatively and non-invasively. In Eq. (1), which is valid for a non-magnetic specimen, x and y are directions in the plane of the specimen, normal to the electron beam direction z, C_E is an interaction constant that takes a value of 6.53×10^6 rad V^{-1} m^{-1} at 300 kV, and $V(x,y,z)$ is the electrostatic potential within and around the specimen. In our experiment, we concentrate on the potential in the vacuum region surrounding the W tip.

The off-axis electron holography results that are presented below were acquired at an accelerating voltage of 300 kV using an FEI Titan 80–300ST field emission gun TEM, which is equipped with a Lorentz lens, an electron biprism, a Gatan imaging filter, and a 2048 pixel charge-coupled device camera. The microscope objective lens was switched off and the sample imaged in magnetic-field-free conditions using the Lorentz lens (not shown in Fig. 1(b)) as the primary imaging lens focused on the specimen. A positive voltage was applied to the biprism to generate a set of ~2.5 nm interference fringes in the image plane, resulting in a ~1 μm holographic overlap width (referred to the specimen plane). Vacuum reference holograms were acquired and used to remove distortions associated with the imaging and recording system of the microscope.[16] A mask with radius

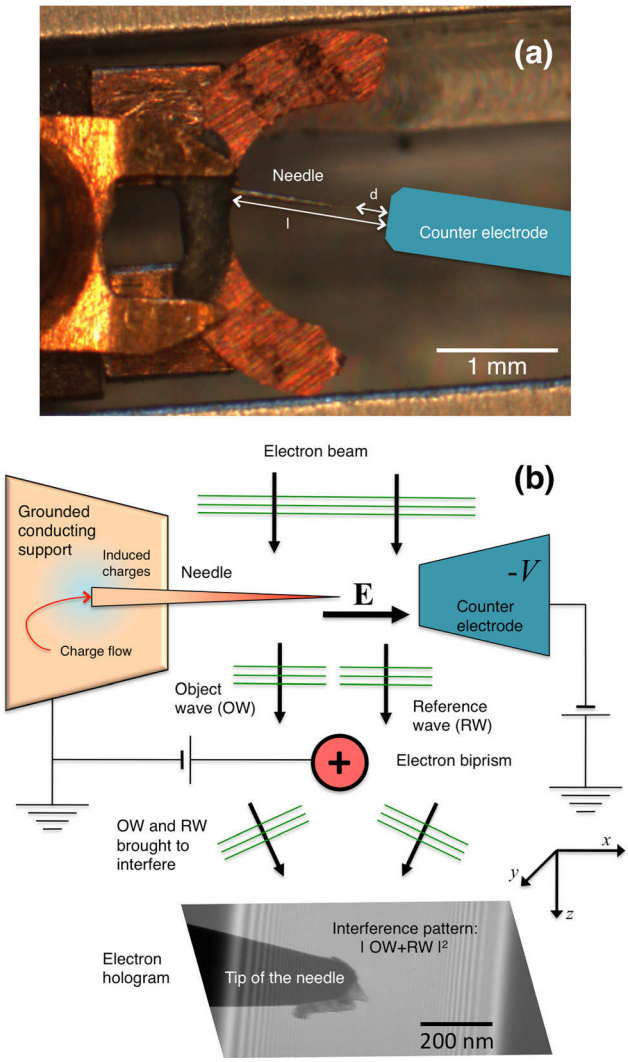

FIG. 1. (a) Photograph of experimental setup used to record off-axis electron holograms and Fresnel (out-of-focus) images of an etched W tip *in situ* in the TEM. The tip is attached to a Cu TEM grid and clamped in a three-contact cartridge-based specimen holder. A voltage is applied between the tip and a moveable Au counter-electrode at a distance $l = 0.981$ mm from the base of the needle and $d = 11.4$ μm from its tip. (b) Schematic diagram showing the setup used to record off-axis electron holograms of the biased tip. The electron biprism, which is biased at 170 V, is used to overlap the object wave (OW), which has travelled through the region of interest at the end of the needle, with a vacuum reference wave (RW), resulting in ~2.5 nm fringes. A representative experimental electron hologram is shown at the bottom of the figure.

0.2 nm^{-1} was used in reconstructing the hologram, resulting in a nominal spatial resolution of 5 nm.

Figure 2 shows an off-axis electron hologram of the end of the W tip, recorded before a bias was applied to it, alongside reconstructed 2× amplified phase images corresponding to bias voltages of 0, 10, and 20 V, respectively. Since the majority of the electrons that impinge on the tip are scattered to high angles and removed from the beam path, we assume below that the amplitude of the object transmission function has values of 0 in the tip and 1 surrounding it.

The images in Fig. 2 show a region of contamination or dirt on the tip, which perturbs both the amplitude and the phase slightly. However, its presence does not affect the

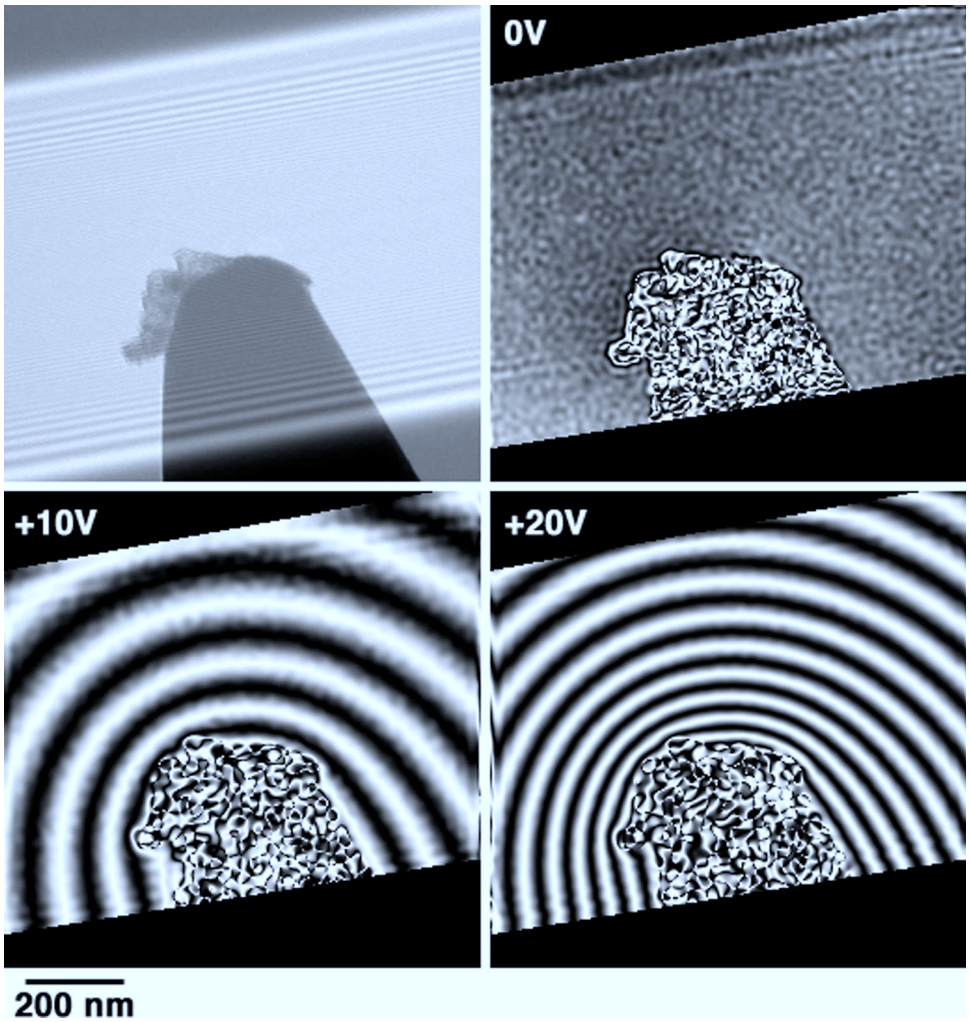

FIG. 2. Off-axis image-plane electron hologram of the unbiased W tip (top left), shown alongside reconstructed 2× amplified phase images recorded for applied bias voltages of 0, 10, and 20 V, for a distance to the Au counter-electrode of 11.4 μm.

primary conclusions that we obtain from the holographic and out-of-focus observations below. In out-of-focus images of the tip, the effect of the region of contamination on the images was more significant at lower defocus values. Therefore, only one image recorded at a relatively large defocus of ∼6 mm and an applied potential of 90 V, which is shown in Fig. 3, was analysed in detail. This image takes the form of a spectacular caustic in which the overlap of waves from either side of the tip gives rise to a rich system of straight and curved diffraction and interference fringes. The region within the white square shown in Fig. 3 (of side 0.5 μm) was compared with simulations in detail below.

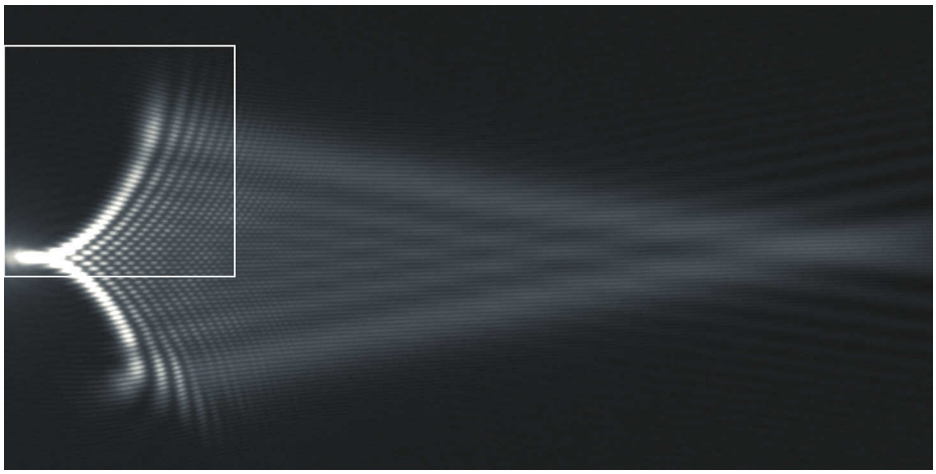

FIG. 3. Experimental image of the W tip recorded approximately 5 mm out of focus without using an electron biprism (see text for details). The pattern of interference fringes results from overlap of waves from either side of the tip. The white square of side 0.5 μm indicates the region that was compared in detail with simulations.

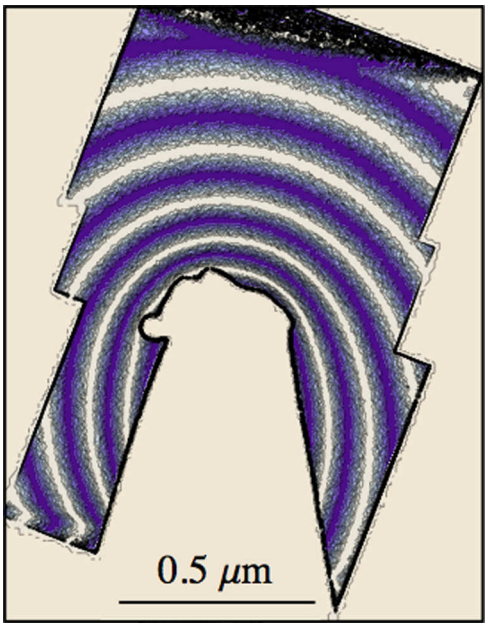

FIG. 4. Reconstructed phase image similar to those shown in Fig. 2, obtained by cutting and pasting together phase images recorded from several holograms, taken at a bias of 20 V, to obtain a larger field of view in the final contour map. The phase contours can now be observed to enter the tip. Amplification factor 1×.

In Fig. 2, the equiphase lines in the contour maps have a density that is proportional to the applied potential and appear to follow the shape of the tip. However, when several phase images are recorded by changing the relative position of the tip and the biprism and pasted together, as shown in Fig. 4, the phase contours are observed to enter the tip over a larger field of view, in contradiction to the simplistic view of phase contours representing equipotential lines.[17,18] The fact that the contours enter the tip results from two fundamental reasons: (i) According to Eq. (1), the phase shift is a projection of the three-dimensional electrostatic potential along the beam direction. However, a projection does not coincide with a cross-section of the potential being projected, unless the potential does not depend on the direction along which it is projected, i.e., $V = V(x,y)$; (ii) Whenever the potential is not strictly bounded within a finite domain, its tails will perturb the region where the vacuum reference wave travels, making it non-planar.[17–19]

Here, as a result of the fact that the vacuum reference wave is perturbed by the stray field from the tip, rather than retrieving the ideal object wavefunction

$$\psi(x,y) = A(x,y)e^{i[\varphi(x,y)]}, \tag{2}$$

electron holography yields information about a fictitious object whose wavefunction is given by the expression

$$\psi(x,y) = A(x,y)e^{i[\varphi(x,y)-\varphi(x+D\cos\theta, y+D\sin\theta)]}, \tag{3}$$

where θ is the angle of the biprism axis with respect to the object and D is the interference distance,[20] which is directly proportional to the biprism potential[15] and should not be confused with the interference field (overlap) width, which also depends on the finite diameter of the electron biprism wire. See Refs. 18 and 19 for details and diagrams. The value of D can be measured by recording two interferograms at different biprism potentials and measuring the variation in distance between recognizable features.

In general, the problem of removing the effect of a perturbed reference wave from a single recorded electron hologram is unsolved[21] and the only way to access quantitative information from a single phase image is to compare the measured phase shift with a sound physical model of the field under investigation. Alternatively, the effect of the perturbed reference wave can be minimised by increasing the interference distance, for example, by using a TEM equipped with two or three biprisms, one of which is in the condenser lens system of the microscope.[22]

The fact that an off-axis electron hologram captures the phase difference between an object and a reference wave also has some advantages, one of which is related to the contribution to the phase shift from the externally applied field E. Its extension is finite and unspecified, as it depends on the overall boundary conditions (primarily the shape and distance of the Au counter-electrode used to bias the object), but its contribution to the phase shift corresponds to an unknown linear term, which becomes less troublesome when the phase difference is considered. As will be shown below, a similar conclusion also holds for astigmatic contributions to the phase shift, which are quadratic and so do not affect the holographic difference image substantially, apart from unimportant linear terms, whereas they cannot be overlooked as easily in out-of-focus observations.

III. THEORETICAL MODEL

The first electron holographic observations of biased metallic tips were interpreted on the basis of a simple model, comprising a line of charges in front of a grounded conducting plane.[17] If the charge density is constant, then the potential distribution and the corresponding electron-optical phase shift are computable in analytical form using image charge methods. As the equipotential surfaces around such a charge distribution resemble ellipsoids, which are in turn similar to the physical shape of the tip itself, a line of charges generates a suitable solution for the electrostatic field in the region surrounding such a tip. By tuning the value of the charge density to generate an equipotential that matches the actual tip shape, satisfactory agreement could be reached between theory and experiment.[17]

However, this early model is insufficient to represent an experimental setup in which a needle is subjected to an external electric field. In order to tackle this problem, several analytical models have been developed, as summarized in the appendix of Ref. 23. The most suitable of the models for our purpose is the hyperboloid or semi-ellipsoid model in which a solution for the potential and the field can be obtained in the prolate-spheroidal coordinate system.[24–29]

A simpler derivation of the same result can be obtained by considering the field that is generated by a linear distribution of charges, whose density increases linearly along its length.[24,30] The electron-optical phase shift can also be calculated easily in this case. It is useful to outline this derivation, starting from the electrostatic potential of two opposite point

charges $\pm dq$ located at the variable coordinates $(0, \pm t, 0)$ in a Cartesian system (x, y, z), with the z-axis parallel to and in the same direction as the electron beam, in the form

$$dV(r,z) = \frac{dq}{4\pi\epsilon_0}\left(\frac{1}{\sqrt{r^2+(y-t)^2}} - \frac{1}{\sqrt{r^2+(y+t)^2}}\right), \quad (4)$$

where $r = \sqrt{x^2+z^2}$ and the charge located at $y = -t$ is an image charge representing the effect of a conducting grounded planar electrode located on the (x, z) plane. The corresponding electron-optical phase shift is given by the expression

$$d\varphi(x,y) = \frac{dqC_E}{4\pi\epsilon_0}\left\{\log[x^2+(y+t)^2] - \log[x^2+(y-t)^2]\right\}. \quad (5)$$

If the charge density is now assumed to vary linearly along y from $-L$ to L according to the expression $dq = Kt\,dt$, where K is an appropriate constant with units of surface charge density, then the potential and the phase shift can be expressed analytically in the forms

$$V(r,z) = -\frac{Ky}{4\pi\epsilon_0}\left(\frac{4L}{\sqrt{r^2+(y-L)^2}+\sqrt{r^2+(y+L)^2}} + \log\frac{\sqrt{r^2+(y-L)^2}+(y-L)}{\sqrt{r^2+(y+L)^2}+(y+L)}\right) \quad (6)$$

and

$$\varphi(x,y) = \frac{KC_E}{8\pi\epsilon_0}\left\{4Ly + 4xy\arctan\left[\frac{y-L}{x}\right] - 4xy\arctan\left[\frac{y+L}{x}\right] - \left(L^2+x^2-y^2\right)\log\left[\frac{x^2+(y-L)^2}{x^2+(y+L)^2}\right]\right\}, \quad (7)$$

respectively. These expressions can be obtained by elementary means using standard indefinite integrals.[31]

By adding to Eq. (6) the potential $-Ey$ corresponding to a constant electric field $\mathbf{E} = E\hat{\mathbf{y}}$, we find that the shape of the metallic tip is given by the solution of the equation for the zero-potential surface

$$V(r,z) - Ey = 0, \quad (8)$$

which, following Refs. 24 and 30 by introducing the new coordinates $r_+ = \sqrt{r^2+(y+L)^2}$ and $r_- = \sqrt{r^2+(y-L)^2}$ and using the identity $4Ly = r_+^2 - r_-^2$, can be rewritten in the form

$$-\frac{4L}{r_+ + r_-} + \log\left(\frac{r_+ + r_- + 2L}{r_+ + r_- - 2L}\right) = \frac{4\pi\epsilon_0 E}{K}. \quad (9)$$

This equation is satisfied by an ellipsoid of revolution (a spheroid) of the form $r_+ + r_- = 2a$, which has foci at $(0, -L, 0)$ and $(0, L, 0)$ and major semi-axis a, so long as

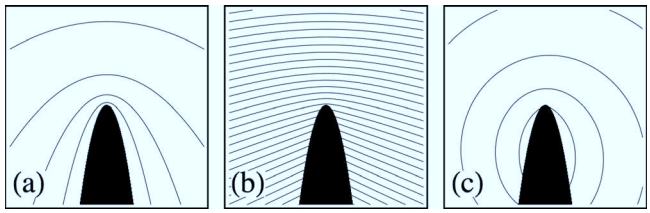

FIG. 5. (a) Tip (dark) and equipotential surfaces surrounding it, with a spacing of 1 V, based on the model described in the text, for input values of $a = 0.97$ mm, $b = 6.25\,\mu$m, and $E \approx 10.2$ kV/m. (b) Corresponding equiphase lines and (c) perturbed equiphase lines, with a spacing of 2π radians, for an interference distance $D = 1\,\mu$m at an angle $\theta = 8°$. The side of each square region is $2\,\mu$m.

$$E = \frac{K}{4\pi\epsilon_0}\left(\log\frac{1+e}{1-e} - 2e\right), \quad (10)$$

where $e = L/a$ is the eccentricity of the ellipsoid. Therefore, any arbitrary prolate ellipsoid with a given eccentricity $0 < e < 1$ can be made equipotential by choosing the appropriate value of the ratio E/K according to Eq. (10).

Figure 5(a) shows a simulation of the shape of the tip (elliptic null equipotential) and equipotential contours with a spacing of 1 V surrounding it, for a square region of side $2\,\mu$m. The geometrical input data have been taken from the macroscopic parameters, i.e., major semi axis $a = 0.97$ mm and minor semi-axis $b = 6.25\,\mu$m, whereas a value of $E \approx (10/0.98)$ V/mm ≈ 10.2 kV/m was chosen for the field, for the sake of illustration, in spite of the different boundary conditions in the experimental setup shown in Fig. 1(a) compared to the planar model shown in Fig. 1(b). It is interesting to note the difference between this image (Fig. 5(a)) and the trend of the corresponding equiphase lines with $\Delta\varphi = 2\pi$ rad, shown in Fig. 5(b), as well as the dramatic difference, both in shape and in contour line density, when the perturbed reference wave is taken into account, as shown in Fig. 5(c). The interference distance has been taken to be $D = 1\,\mu$m at an angle of $\theta = 8°$.

IV. INTERPRETATION OF EXPERIMENTAL RESULTS

In order to extract quantitative information from the experimental measurements, we first fit the outer shape of the tip, as seen in projection, to an ellipse. For major semi-axis a, we choose the length of the needle, which is measured to be 0.97 mm. In order to choose a value for the minor semi-axis b, we varied its value until a best-fitting value was obtained for the largest available field of view (Fig. 4). We obtained a value of $b = 7.42\,\mu$m, which agrees reasonably well with the measured value of the needle radius near the grounded plate ($6.25\,\mu$m), suggesting that the needle is close to ellipsoidal in shape, as shown in Fig. 6.

Having determined the shape of the needle, a value for K can be determined from a best fit to the phase image over the full composite field of view. Figure 7 shows that very good agreement is obtained for a value of $K = 1.76 \times 10^{-19}$ C/μm^2, corresponding to 1.1 electrons/μm^2. The corresponding value for the parameter E, according to Eq. (10), is 15 kV/m, which is comparable to the electric

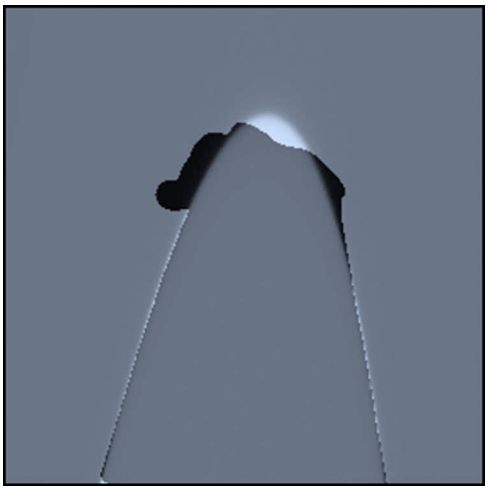

FIG. 6. Best fit of the tip shape parameters carried out to determine the major and minor semi-axes of the ellipsoidal null equipotential. The side of the square region is 1 μm.

field $E = 20.4\,\text{kV/m}$ generated by a potential difference of 20 V applied to two flat-plate electrodes 0.97 mm apart.

Insertion of the figures obtained from the best fit to the experimental data into the model can now be used to provide the topography of the field around the tip. Figure 8 shows a map of (a) the electric field intensity and (b) its profile at the surface, evaluated along the dashed line in (a). The 20 V bias applied to the needle generates an electric field at its apex of $E_{\text{apex}} = 82.1$ MV/m. The ratio E_{apex}/E corresponds to a field enhancement factor relative to two flat plates of close to 5500. This value agrees well with the usual expression for the electric field at the apex of a sharp needle[3,32]

$$E_{\text{apex}} = \frac{V}{kR} \tag{11}$$

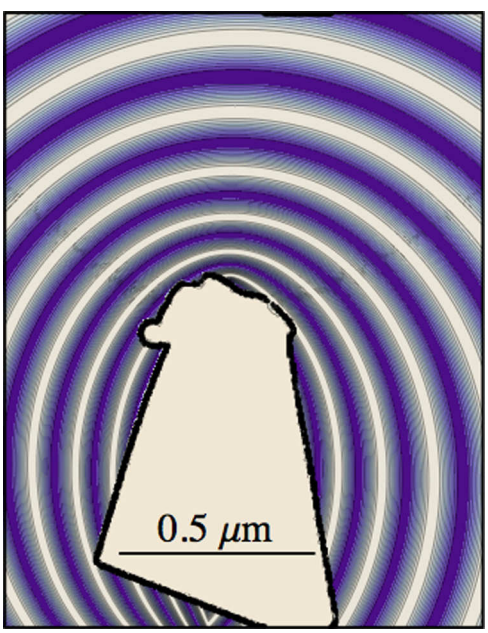

FIG. 7. Best-fitting phase image simulation to the experimental measurements of Fig. 4, corresponding to a value for E of 15 kV/m, with the true tip outline extracted from the experimental image superimposed. Amplification factor 1×.

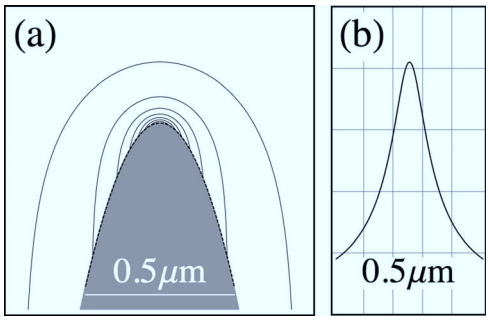

FIG. 8. (a) Plot of the electric field intensity around the tip for a single line charge. The contour spacing is 10 MV/m. (b) Electric field intensity profile along the dashed line in (a). The vertical separation of the grid lines is 20 MV/m.

and gives a value for k of 2.5 for $R = 150\,\text{nm}$, where k is the field enhancement factor and R is the radius of curvature of the tip apex. This value for k is very close to the usual value of 3 valid for a metallic half-sphere.[30]

In Fig. 6, the main differences between the model and the experiment are at the very top of the tip. As the tip is slightly flattened, we improved our simple model by considering three laterally displaced line charges instead of one, at a distance of 50 nm from each other, each carrying (1/3) of the original charge. In this way, we could model a slightly flattened tip, as shown in Fig. 9(a), with a strong variation of the field across the tip. There is, however, no dramatic change in the average electric field along the dashed line at its surface, as shown in Fig. 9(b), indicating that the foregoing considerations are still substantially valid.

V. OUT-OF-FOCUS OBSERVATIONS

A convincing proof of the soundness of the procedure outlined above is provided by using the measured quantities as input for an independent simulation of Fresnel images recorded from the same specimen, such as that shown in Fig. 3. Out-of-focus image simulations were carried out by calculating the Fresnel-Kirchhoff diffraction integral[33] by means of Fast Fourier Transform algorithms.

In order to interpret the most relevant features in this image, we first focused our attention on the boxed region, shown in Fig. 3, where the fringes are less disturbed by the presence of the impurity. In order to limit the number of free

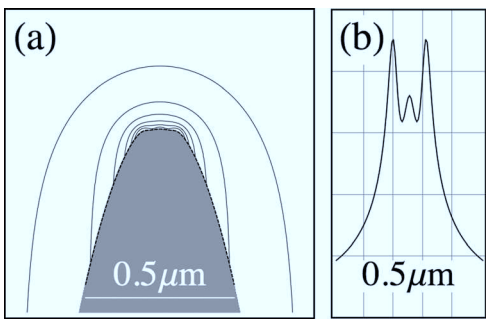

FIG. 9. (a) Plot of the electric field intensity around the tip for three line charges charge. The contour spacing is 10 MV/m. (b) Electric field intensity profile along the dashed line in (a). The vertical separation of the grid lines is 20 MV/m.

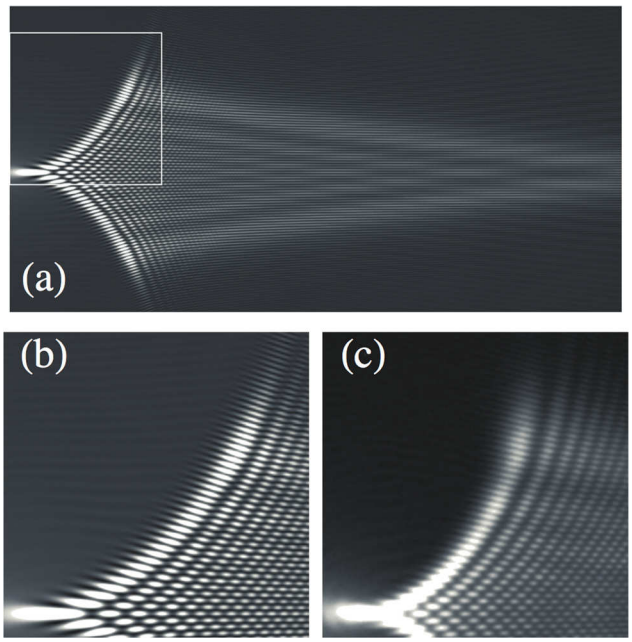

FIG. 10. (a) Theoretical out-of-focus image of the tip, for a defocus distance of 5 mm and a field E corresponding to a tip bias of 90 V. The white boxed area shown in (b) is compared with the corresponding region (c) of the experimental out-of-focus image shown in Fig. 3.

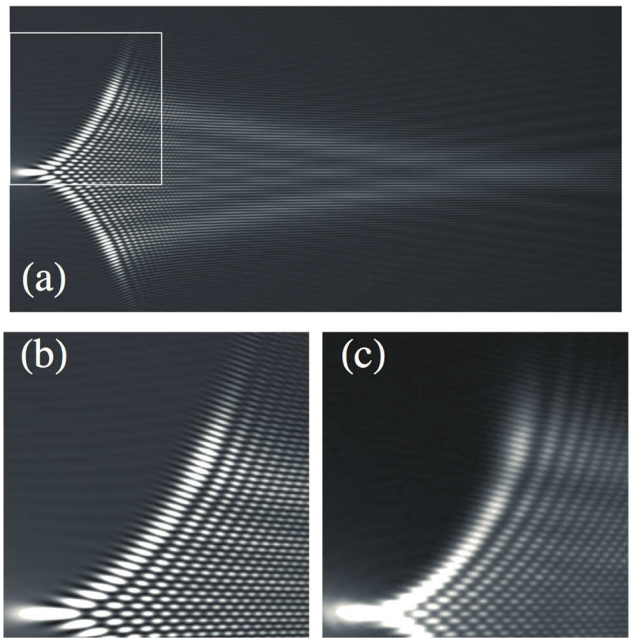

FIG. 11. (a) Simulated out-of-focus image of the tip including astigmatism. The white boxed area (b) is compared with the corresponding region (c) of the experimental out-of-focus image shown in Fig. 3.

parameters, we refined the defocus by comparing the experimental image taken at an applied voltage of 0 V with that calculated using the geometric parameters obtained from the holographic best fit, obtaining 5 mm for the defocus. Figure 10(a) shows a simulation of an out-of-focus image of the tip for an applied potential of 90 V. The simulation shows overall qualitative agreement with the experimental image shown in Fig. 3. However, it differs in several details, such as in the bending of the two wings (which cannot be explained by an error in defocus) and in the spacing of the interference fringe systems. These differences are better revealed by comparing the boxed region in the simulation shown in Fig. 10(b) with the corresponding region extracted from the experimental image shown in Fig. 10(c).

We established that the rounding of the tip (described using the multi-wire model discussed in Sec. IV) is not responsible for these discrepancies. We then reconsidered the setup in order to find a reasonable explanation, concluding eventually that the half-cylindrical shape of the aperture supporting the tip results in an electric field near the tip region that can be approximately described using a cylindrical capacitor topography, giving a logarithmic potential in the radial coordinate. Considering a field of the form $\log\sqrt{x^2+y^2}$ and expanding it in a Taylor series around the tip, the second order terms in the phase shift correspond to those of an astigmatic lens, whose phase is given by the expression

$$\frac{\pi}{\lambda}\left(\frac{x^2}{f}-\frac{y^2}{f}\right). \tag{12}$$

If this additional term is inserted into the simulations, then the difference between theory and experiment is greatly reduced, as shown in Fig. 11, where the parameter f was varied in order to improve the agreement in the boxed region. Figure 11(a) shows the whole image simulated for a value of $f = 60$ mm, whereas Figs. 11(b) and 11(c) show the boxed area for the simulated and experimental images, respectively. A more quantitative comparison is shown in Fig. 12, in the form of (a) the experimental and simulated line scans across the central symmetry axis and (b) a superposition of the theoretical contour image (one contour) with the experimental image.

The overall satisfying agreement, both locally and globally, confirms the soundness of our hypothesis and suggests that the topography of the applied field should be considered carefully when using out-of-focus images as a complement to electron holographic observations. As previously mentioned, the quadratic phase factors in Eq. (12), which are related to astigmatism, do not influence the holographic phase difference image significantly, as they give rise to unessential linear phase factors, which are not important for the fitting procedures described above. This is another

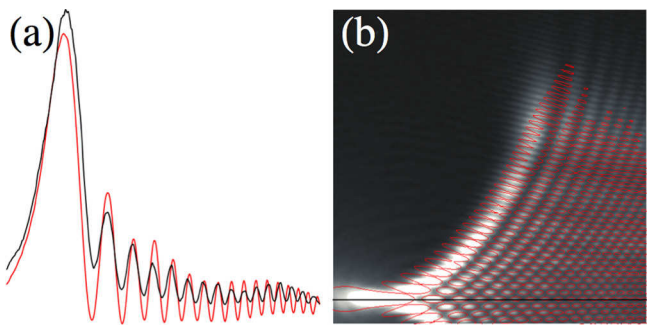

FIG. 12. Comparison of experimental and simulated images including astigmatism. In (a) are shown the experimental (black) and simulated (red) line scans extracted from the central symmetry axis of the out-of-focus image (dark horizontal line in (b)), while (b) shows the simulated contour map overlaid onto the experimental image.

advantage of the holographic method when compared with the out-of-focus technique.

Although out-of-focus images are highly spectacular in this case, it is in general difficult to obtain quantitative information from them because: (i) The relationship between phase shift and Fresnel image intensity is non-linear; (ii) the calibration of the microscope under the conditions that are used is troublesome, since the defocus values indicated by the instrument may not be reliable; (iii) the effect of spherical illumination on defocus should be taken into account,[34] as well as the partial coherence of the electron beam, not to mention, as shown here, the presence of astigmatism introduced by the geometry of the applied electric field.

VI. CONCLUSIONS

We have shown that a combination of off-axis electron holography and theoretical modelling can be used to obtain quantitative information about the electric field around the tip of a biased metallic needle. We have also shown how the model can be modified to take into account more general shapes of the tip. With respect to previous modelling based only on the tip shape, electron holography allows the field around the tip to be measured quantitatively in an experimental electron microscopy setup. Comparison with out-of-focus experiments suggests the presence of astigmatism, which is likely to be due to the geometry of the applied electric field, but does not affect the holographic observations substantially. The next steps is, on the theoretical side, to improve the best fit by using more sophisticated models in order to take into account more complex shapes of the tip,[2,35] including those without rotational symmetry. On the experimental side, it may be useful to vary the tilt around the needle axis in order to gain information about the three-dimensional nature of the electric field directly, as well as to increase the bias of the counter-electrode until field emission is triggered, in order to obtain a more complete understanding of the field emission process. Regarding out-of-focus observations, careful attention should be paid to the calibration of the electron-optical setup, as well as to the design of the specimen stage, in order to avoid or minimize the observed astigmatic contribution to the phase of the electron wavefunction.

A few final remarks concerning similar research efforts by others. In this work, we have chosen analytical modelling over a numerical approach based on finite element methods[36,37] for the interpretation of the experimental results. However, we believe that a combination of the two methods is necessary in order to highlight and avoid the respective pitfalls. We should also mention that similar experiments to ours have been carried out using low energy electron point source (LEEPS) microscopy, also named electron projection microscopy (EPM), point projection microscopy (PPM), or kendroscopy (see Ref. 38 and references therein). The imaging method used in this instrument is in-line holography, which is severely affected by the presence of charges in the imaged object.[38,39] Although two-beam interference experiments have been carried out by inserting a biased wire,[40] a charged carbon fiber,[41] or a carbon nanotube,[42] no results comparable with those in the holographic TEM have been achieved so far, except for a measurement of the coherence of the beam.[41,42] Finally, direct model-independent information about the value of the charge density in the tip region may be obtained by applying the method introduced in Ref. 43 to measure and localize charges by making use of Gauss' law. Unfortunately, the thickness of the tip interior reduces the holographic fringe contrast in the present experiment to the point that it becomes opaque to the electrons, so that the application of the method may not be straightforward.

ACKNOWLEDGMENTS

The authors are grateful to A. Cerezo for valuable discussions. G.P. is grateful to the Udenlandske Gæsteprofessorater program of the Otto Mønsted Foundation for supporting his research stay at the Technical University of Denmark. R.D.B. acknowledges the European Commission for an Advanced Grant and the Deutsche Forschungsgemeinschaft for a Deutsch-Israelische Projektkooperation (DIP) Grant.

[1]T. Kasama, Y. Antypas, R. K. K. Chong, and R. E. Dunin-Borkowski, MRS Online Proc. Libr. **839**, P5.1 (2004).
[2]D. L. Jaeger, J. J. Hren, and V. V. Zhirnov, J. Appl. Phys. **93**, 691 (2003).
[3]M. K. Miller, A. Cerezo, M. G. Hetherington, and G. D. W. Smith, *Atom Probe Field Ion Microscopy* (Clarendon Press, Oxford University Press, Oxford, 1996).
[4]T. F. Kelly and M. K. Miller, Rev. Sci. Instrum. **78**, 031101 (2007).
[5]T. F. Kelly, M. K. Miller, K. Rajan, and S. P. Ringer, Microsc. Microanal. **19**, 652 (2013).
[6]T. F. Kelly, E. Voelkl, and B. P. Geiser, Microsc. Microanal. **15**, 12 (2009).
[7]M. P. Moody, B. Gault, L. T. Stephenson, D. Haley, and S. P. Ringer, Ultramicroscopy **109**, 815 (2009).
[8]D. J. Larson, B. P. Geiser, T. J. Prosa, and T. F. Kelly, Microsc. Microanal. **18**, 953 (2012).
[9]R. Smith and J. Walls, J. Phys. D: Appl. Phys. **11**, 409 (1978).
[10]S. T. Loi, B. Gault, S. P. Ringer, D. J. Larson, and B. P. Geiser, Ultramicroscopy **132**, 107 (2013).
[11]T. Kasama, R. E. Dunin-Borkowski, L. Matsuya, R. F. Broom, A. C. Twitchett, P. A. Midgley, S. B. Newcomb, A. C. Robins, D. W. Smith, J. J. Gronsky, C. A. Thomas, and P. E. Fischione, MRS Online Proc. Libr. **907E**, MM13.2 (2005).
[12]A. Tonomura, *Electron Holography* (Springer, Berlin, 1993), Vol. 70.
[13]R. E. Dunin-Borkowski, M. R. McCartney, and D. J. Smith, *Electron Holography of Nanostructured Materials*, The Encyclopaedia of Nanoscience and Nanotechnology Vol. 3 (American Scientific Publishers, 2004), pp. 41–100.
[14]H. Lichte and M. Lehmann, Rep. Prog. Phys. **71**, 016102 (2008).
[15]G. Möllenstedt and H. Düker, Z. Phys. **145**, 377 (1956).
[16]M. Lehmann and H. Lichte, Microsc. Microanal. **8**, 447 (2002).
[17]G. Matteucci, G. F. Missiroli, M. Muccini, and G. Pozzi, Ultramicroscopy **45**, 77 (1992).
[18]G. Matteucci, G. F. Missiroli, and G. Pozzi, in *Advances in Imaging and Electron Physics*, edited by P. W. Hawkes (Elsevier, 2002), Vol. 122, pp. 173–249.
[19]G. Matteucci, G. Missiroli, E. Nichelatti, A. Migliori, M. Vanzi, and G. Pozzi, J. Appl. Phys. **69**, 1835 (1991).
[20]G. F. Missiroli, G. Pozzi, and U. Valdrè, J. Phys. E: Sci. Instrum. **14**, 649 (1981).
[21]D. Van Dyck, J. Electron Microsc. **48**, 33 (1999).
[22]T. Tanigaki, Y. Inada, S. Aizawa, T. Suzuki, H. S. Park, T. Matsuda, A. Taniyama, D. Shindo, and A. Tonomura, Appl. Phys. Lett. **101**, 043101 (2012).
[23]S. Belaidi, P. Girard, and G. Leveque, J. Appl. Phys. **81**, 1023 (1997).
[24]E. Durand, *Électrostatique* (Masson, Paris, 1964), Vol. 2.
[25]J. D. Nordgard, J. Appl. Phys. **48**, 3042 (1977).

[26]L.-H. Pan, T. E. Sullivan, V. J. Peridier, P. H. Cutler, and N. M. Miskovsky, Appl. Phys. Lett. **65**, 2151 (1994).
[27]J. D. Zuber, K. L. Jensen, and T. E. Sullivan, J. Appl. Phys. **91**, 9379 (2002).
[28]K. L. Jensen, D. W. Feldman, and P. G. O'Shea, J. Vac. Sci. Technol., B **23**, 621 (2005).
[29]L.-H. Pan, V. J. Peridier, and T. E. Sullivan, Phys. Rev. B **71**, 035345 (2005).
[30]E. G. Pogorelov, A. I. Zhbanov, and Y.-C. Chang, Ultramicroscopy **109**, 373 (2009).
[31]I. S. Gradshteĭn, I. M. Ryzhik, and A. Jeffrey, *Table of Integrals, Series, and Products*, 7th ed. (Academic Press, Boston, 2007).
[32]R. Gomer, *Field Emission and Field Ionization* (Harvard University Press Cambridge, MA, 1961), Vol. 34.
[33]M. Born and E. Wolf, *Principles of Optics: Electromagnetic Theory of Propagation, Interference and Diffraction of Light*, 4th ed. (Pergamon Press, Oxford, 1969).
[34]P. F. Fazzini, P. G. Merli, and G. Pozzi, Ultramicroscopy **99**, 201 (2004).
[35]G. Mesa, E. Dobado-Fuentes, and J. J. Saenz, J. Appl. Phys. **79**, 39 (1996).
[36]J. Kim, W. Xia, D. Shindo, T. Oikawa, and T. Tomita, Mater. Trans. **48**, 2631 (2007).
[37]T. Oikawa, J. J. Kim, T. Tomita, H. S. Park, and D. Shindo, J. Electron Microsc. **56**, 171 (2007).
[38]A. Beyer and A. Gölzhäuser, J. Phys.: Condens. Matter **22**, 343001 (2010).
[39]V. Georges, J. Bardon, A. Degiovanni, and R. Morin, Ultramicroscopy **90**, 33 (2001).
[40]R. Morin and A. Degiovanni, J. Vac. Sci. Technol., B **13**, 407 (1995).
[41]B. Cho, T. Ichimura, R. Shimizu, and C. Oshima, Phys. Rev. Lett. **92**, 246103 (2004).
[42]J. Y. Mutus, L. Livadaru, R. Urban, J. Pitters, A. P. Legg, M. H. Salomons, M. Cloutier, and R. A. Wolkow, New J. Phys. **15**, 073038 (2013).
[43]M. Beleggia, T. Kasama, R. E. Dunin-Borkowski, S. Hofmann, and G. Pozzi, Appl. Phys. Lett. **98**, 243101 (2011).